Metallic and molecular orbital concepts in XMg8 clusters, X = Be-F

Victor M. Medel, Arthur C. Reber, J. Ulises Reveles, and Shiv N. Khanna

Citation: J. Chem. Phys. **136**, 134311 (2012); doi: 10.1063/1.3700086
View online: http://dx.doi.org/10.1063/1.3700086
View Table of Contents: http://jcp.aip.org/resource/1/JCPSA6/v136/i13
Published by the American Institute of Physics.

Metallic and molecular orbital concepts in XMg_8 clusters, X = Be-F

Victor M. Medel, Arthur C. Reber, J. Ulises Reveles, and Shiv N. Khanna[a)]
Department of Physics, Virginia Commonwealth University, Richmond, Virginia 23284, USA

(Received 3 February 2012; accepted 15 March 2012; published online 3 April 2012)

The electronic structure and stability of the XMg_8 clusters (X = Be, B, C, N, O, and F) are studied using first principles theoretical calculations to understand the variation in bonding in heteroatomic clusters which mix simple divalent metals with main group dopants. We examine these progressions with two competing models, the first is a distorted nearly free electron gas model and the second is a molecular orbital picture examining the orbital overlap between the dopant and the cluster. OMg_8 is found to be the most energetically stable cluster due to strong bonding of O with the Mg_8 cluster. $BeMg_8$ has the largest HOMO-LUMO gap due to strong hybridization between the Mg_8 and the Be dopant states that form a delocalized pool of 18 valence electrons with a closed electronic shell due to crystal field effects. Be, B, and C are best described by the nearly free electron gas model, while N, O, and F are best described through molecular orbital concepts. © *2012 American Institute of Physics*. [http://dx.doi.org/10.1063/1.3700086]

I. INTRODUCTION

Localized and delocalized concepts[1] for an intuitive understanding of the interactions between atoms in molecules, clusters, and bulk materials provide insight into the electronic structure and stability of chemical species; however, choosing and contrasting the appropriate conceptual model is one of the central challenges of quantum chemistry. Simple metal clusters are positioned at one extreme of the spectrum of delocalized systems as their physics is explained through a jellium model in which the electrons are treated as metallic or more precisely as a confined nearly free electron (NFE) gas.[2–4] A second framework through which chemical stability is understood is molecular orbital theory in which bonding and antibonding orbitals reveal the stability, which lies closer to the localized view of bonding and is exemplified by the covalent bonding between elements with $2p$ valence electrons.[5,6] Therefore, it is of interest to examine delocalized simple metal clusters with a dopant atom with $2p$ valence electrons (Be-F) to examine the conceptual framework which could offer insight into the cluster's electronic structure and stability. Heteroatomic clusters are a powerful tool for understanding fundamental interactions between metals and dopants, so we choose clusters to serve as our model system.[7–19]

There have been numerous efforts to develop simple "metallic" models that provide qualitative information on the distribution of electronic states and the nature of molecular orbitals in many-atoms systems because calculating the wave function is both a computationally heavy task and the solution does not guarantee physical insight. One-dimensional metallic models were proposed in the first half of the last century to understand highly conjugated molecules in one dimension,[20,21] and three-dimensional models were developed to understand the absorption spectra of decaborane.[22] A metallic "unified atom" model for polyhedral borane clusters was proposed by Hoffman and Lipscomb where the valence electrons of a central site are subjected to a crystal field determined by the effective nuclear charges on surrounding atoms.[23] For tetrahedral, octahedral, and icosahedral symmetries in this model, one obtains filled shells at electron counts of 2, 8, 20, 40, 70, … Such a simplified model, however, does not account for all the observations in metallic systems. For example, Knight and co-workers generated Na_n clusters in beams and found that clusters containing 2, 8, 18, 20, 34, 40, 58, … atoms exhibited enhanced stability and were called magic numbers.[2] They also proposed that the observed magic numbers had an electronic origin that could be accounted for within an effective spherical jellium model in which the positive charges on the ionic cores are smeared into a uniform spherical background determined by the size of cluster. Such a potential leads to bunching of the electronic states which can again be classified by *nl* quantum numbers (1S, 1P, 1D, 2S, …) with closed electronic shells at electron counts 2, 8, 18, 20, 34, 40, 58, 68, 70, 92, … Extensive experimental work on the stability, polarizability, ionization potentials, and reactivity over the past three decades has shown that the spherical jellium model, despite being highly simplistic and marked by indisputable limitations, does provide an overall representation of the observed behaviors.[24–30] This evidence is further supported by first principles studies on symmetric compact clusters that show that the energy ordering and shapes of molecular orbitals conform largely to the ordering suggested by the jellium picture.[31–35]

While the existing experimental evidence on magic species provided evidence for the validity of "metallic" models, the bunching of electronic states led Khanna *et al.* to propose the "superatom" concept.[3] They showed that an Al_{13} cluster with a $2P^5$ highest occupied electronic orbital had a high electron affinity comparable to halogen atoms. Motivated by their findings, they proposed that stable spherical clusters could be regarded as "superatoms" forming a third

a)E-mail: snkhanna@vcu.edu.

dimension to the periodic table. Superatom clusters with an effective chemical valence provided an organizing principle which instructed much of cluster research, and over the past 20 years, numerous superatoms including inert, halogen, multivalent, and magnetic species have been identified.[36–43]

Unlike atoms, the electronic orbitals in superatoms are delocalized over the cluster and hence offer new features. However, like atomic orbitals, the superatomic orbitals have same angular distributions. It is therefore interesting to explore the nature of bonding and hybridization between the superatomic and atomic orbitals. In a recent work, we had examined the magnetic properties of XMg_8 (X = 3*d* transition metals) clusters.[42] The clusters were found to have ground states that correspond to a square antiprism of Mg atoms with an endohedral X atom. Further, we showed that the X atoms induced an exchange splitting of the superatomic shells, leading to the possibility of designing superatoms with magnetic supershells.

Our objective in this work is to examine the hybridization between superatomic delocalized orbitals and atomic 2*p*-states as the atomic states become lower in energy, becoming increasingly localized. We examine this interesting aspect by considering a composite cluster containing 8 Mg and a Be, B, C, O, N, or F dopant atom (2nd row of the periodic table). Since Mg is divalent, an Mg_8 cluster has a valence pool of 16 valence electrons with a $1S^2$, $1P^6$, $1D^8$ configuration with partially occupied 1D superatomic orbitals. The addition of a hetero 2nd row atom/dopant with 2*s* or 2*p* valence states is shown to lead to a progression across the series towards an electronic spectrum that can better described as a unified jellium in the beginning of the series ($BeMg_8$), and that evolves towards a bonding anti-bonding like picture as the atomic *p*-states become more localized at the end of the series (OMg_8).

II. THEORETICAL METHODS

The ground state geometries, one electron states and molecular orbitals of XMg_8 clusters (X = Be, B, C, N, O, and F) were calculated within a gradient corrected density functional theory (DFT) formalism. The molecular orbitals are expressed as a linear combination of Gaussian functions centered at the atomic sites. The actual calculations were performed using the deMon2k code[44] with exchange correlation incorporated via the PBE functional.[45] All electrons were considered using a Double Zeta Valence Polarized basis set (DZVP) and the fitted density was expanded using the GEN-A2 auxiliary function set. The exchange energy and potential were calculated by numerical integration of the orbital density. The clusters' molecular orbitals were assigned subshell distinctions based on the symmetry group of the electronic orbitals whenever possible, and through inspection of the nodes in the calculated wave functions. For each case, several trial geometries were fully optimized without constraints in delocalized internal coordinates,[46] starting with previously found geometries for other clusters as well as those obtained using a genetic algorithm method available in our group. Various possible spin multiplicities were investigated, and the reported results are based on geometry and spin optimized ground states. Supporting information provides the Cartesian coordinates and the ground state geometries (Fig. S1) of isomers with the same spin as the ground state but with the dopant atom inside for the cases of B, C, N, O, and outside for the Be. Figs. S2 and S3, showing the contribution of the *s* and *p* atomic orbitals for X and Mg atoms to the molecular orbitals near highest occupied molecular orbital (HOMO), are also included.[47]

III. RESULTS AND DISCUSSION

Fig. 1 shows the ground state geometry of the XMg_8 clusters which exhibit the lowest possible spin multiplicity. The ground state of $BeMg_8$ is a compact structure that can be described as an oblate square antiprism of Mg atoms with an endohedral Be atom. Note that Be and Mg are isovalent with $2s^2$ and $3s^2$ valence configurations and the cluster has a valence count of 18 electrons. For Boron, containing 1*p*-electron and known for its directional bonding, the geometry is a cage of Mg_8 with B occupying a site above the square face that can be considered as distorted boron capped square antiprism. The CMg_8 and NMg_8 cluster show similar geometries although the atoms are closer to the square face than in B. The OMg_8 exhibits a markedly different structure with the O atom binding to a triangular face of the Mg_8 cage that presents a hexagonal bipyramid structure making the overall structure close to a capped hexagonal bipyramid. Finally, FMg_8 has a pentagonal bipyramid geometry of Mg atoms with a F atom (MgF group) bound to an apex Mg site. For the oblate square antiprism geometries of Fig. 1, the Mg-Mg bond lengths show mild variation from 2.92 to 3.3 Å, and the X-Mg distances to the Mg face decrease from 2.3 to 2.08 Å from B to N. As we will show, these geometrical progressions are signatures of the evolution in the nature of bonding.

Earlier studies on pure Mg_n clusters have shown that while Mg_2 is a weakly bound dimer, the clusters undergo a metallic transition with increasing size.[48] The metallic transition stems from the sp- hybridization, that leads to a filling of the p-states, otherwise unoccupied in the Mg atom. In the present case, as we will show later, the frontier orbitals in mixed clusters have a significant contribution from the Mg p-states. It is then interesting to note that some of the

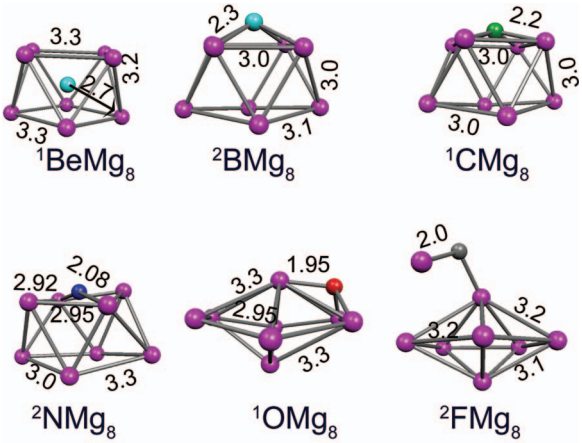

FIG. 1. The ground states geometries of XMg_8. The pink spheres are the Mg atoms and the dopant (X = Be, B, C, N, O, and F) atom is the sphere in different color. The bond lengths are also given in units of Angstroms.

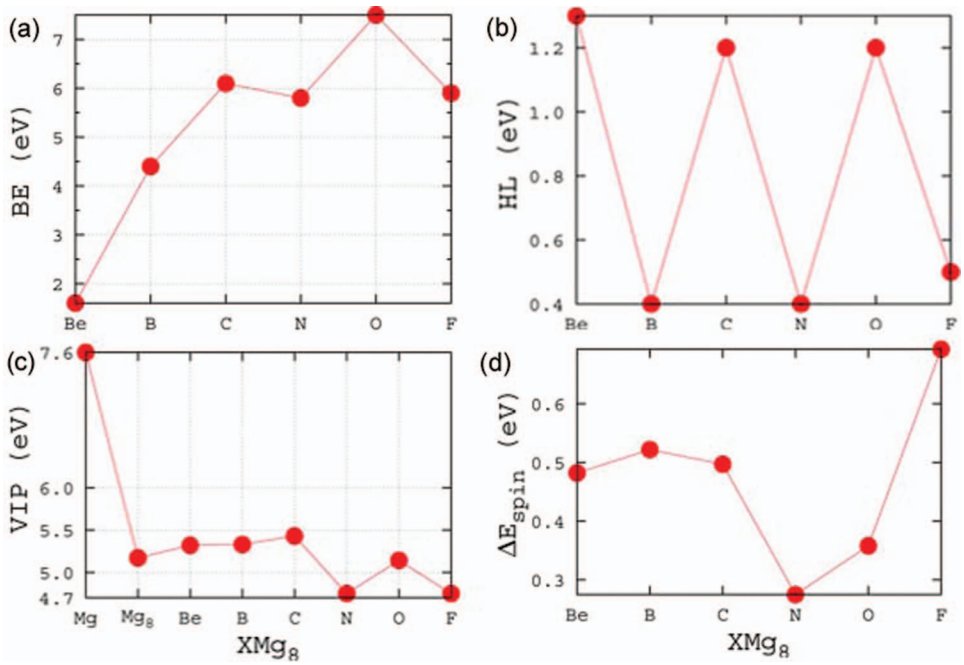

FIG. 2. (a) Trends of binding energy (BE); (b) the HOMO-LUMO gap (HL) for the XMg_8 series; (c) vertical ionization potential (VIP) for Mg, Mg_8, and the XMg_8 series; and (d) variation of spin excitation energy (ΔE_{spin}) for the XMg_8 series.

structures obtained here are similar to those predicted by Wade-Mingos rules,[49–51] often used to rationalize stability of clusters of atoms with p-valence electrons. For example, $BeMg_8$ has an 8-vertex system with 18 (2n + 2) valence electrons. CMg_8 has 9 vertices with 20 (2n + 2) valence electrons. The O site in OMg_8 has two external lone pairs and contributes only two valence electrons. OMg_8 is then an 18 electron valence cluster. The hybridization between s and p orbitals in these metallic clusters makes it difficult to assign "skeletal" electrons,[49–51] so we suspect this correlation is due to a general preference for deltahedral structures. The ground states in many of the clusters are also marked by close lying isomers. These are shown in supplementary Fig. S1 along with the relative energy compared to the ground state.

To monitor the strength of bonding, we calculated the binding energy (BE) of the dopant atom to the Mg_8 cluster via the equation:

$$BE = E(X) + E(Mg_8) - E(XMg_8). \quad (1)$$

Here E(X), E(Mg_8), and E(XMg_8) are the total energies of an X atom, Mg_8 cluster, and XMg_n cluster, respectively. The trends in the BE are given in Fig. 2(a). Note that the BE increases with the increase of 2*p* valence electrons of the dopant atom with two local maxima at C (6.05 eV) and O (7.5eV) and two minima for N(5.84 eV) and F(5.9 eV). We also found that the gap between the HOMO and the lowest unoccupied molecular orbital (LUMO) (HL gap) present a zigzag variation as shown in Fig. 2(b). For the Be, C, and O with even number of electrons, the HOMO-LUMO gap is around 1.2 eV, with Be having the largest value of 1.29 eV. For B, N, and F that contain odd number of electrons, the values are around 0.4 eV with FMg_8 having the largest HL gap of 0.54 eV. As our previous work on Al_n^- has shown, clusters with HOMO-LUMO gaps in excess of 1.0 eV are generally resistant towards etching by oxygen due to a large spin energy excitation, and can therefore be relatively inert.[30] In Fig. 2(c) we show the vertical ionization potential (VIP) for a Mg atom, Mg_8 and XMg_8 clusters. The highest VIP of 7.5 eV for the Mg atom is followed by Mg_8 with 5.10 eV. In the XMg_8 series, the VIP increases up until the CMg_8 with 5.43 eV as a maximum, then, for NMg_8 the VIP drop off to around 4.75 eV, increasing once again to 5.14 eV for OMg_8 and finally dropping off to 4.75 eV for FMg_8. To further investigate the cluster's stability towards spin excitations, we calculated the energy difference between the ground state and the closest isomer of different multiplicity defined as the spin excitation energy, ΔE_{spin}, shown in Fig. 2(d) for the XMg_8 series. For the first three (Be, B, and C) this energy has a value of around 0.5 eV, it then drops to 0.3 eV for NMg_8, which means that it is closer to the nearest isomer of different spin, then ΔE_{spin} increases for OMg_8 and FMg_8, that display the highest value of 0.7 eV.

The relatively high VIP's of CMg_8 and OMg_8 are signatures of a closed electronic shell, while the low VIP's of NMg_8 and FMg_8 are due to enhanced stability of the respective cationic NMg_8^+ and FMg_8^+ species. To understand the evolution in electronic structure and to identify closely packed groupings of states of the XMg_8 series as the dopant atom is changed, we have plotted the calculated density of states in Fig. 3. Each electronic level is broadened with a Gaussian of half-width 0.3 eV. We further projected each state to the dopant site and Mg sites. The red and green regions correspond to the contributions of the dopant *s* and *p* states respectively, while the blue regions are the contributions from the Mg states.

As we progress from Be to F, several trends become apparent. First of all, we want to identify clusters which have an electronic structure in which bunches of closely packed

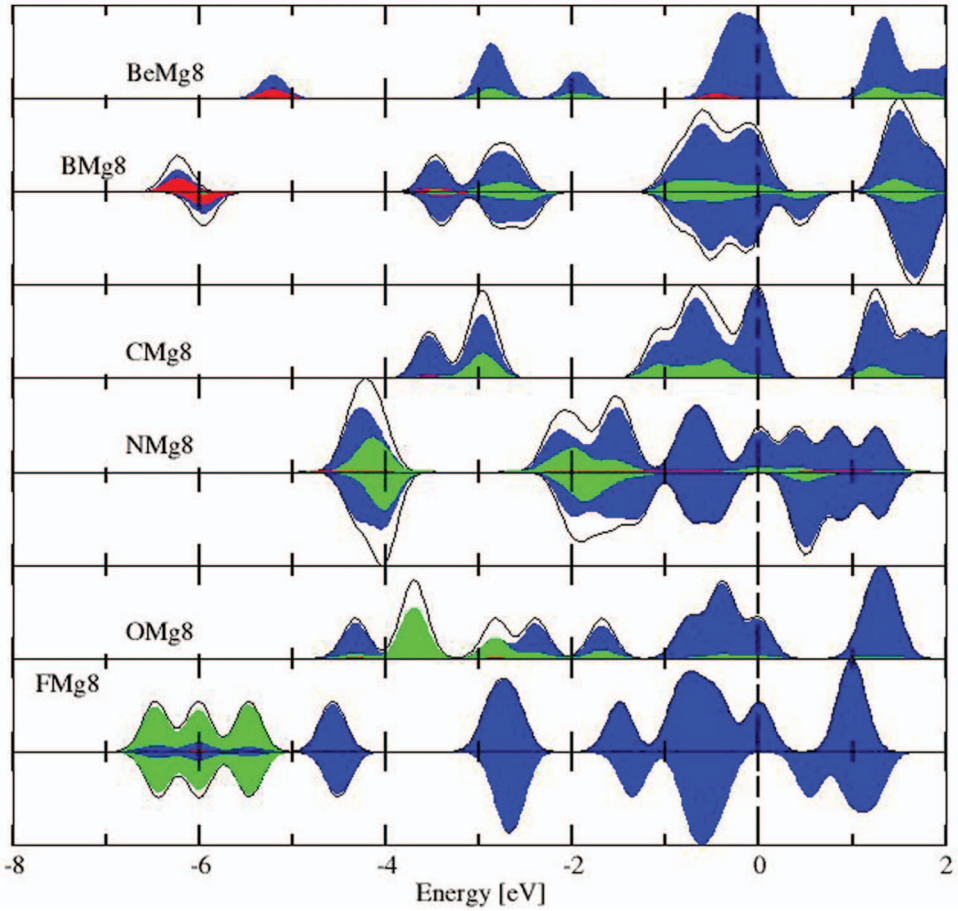

FIG. 3. Density of states of the ground states for XMg_8 series. The red and green colors show the *s* and *p* contribution, respectively, of the dopant atom, while in blue color shows the total contribution of the Mg atoms to molecular states.

levels are separated into well-defined shells. $BeMg_8$ has 4 shells which are well separated from each other, three of which are filled, and a fourth that is unfilled. The shell structure is still visible in BMg_8 and CMg_8, although the shell which contains the HOMO is broadened, and the lowest energy valence shell is lowered in energy because it is controlled by the energy of the 2*s* orbital of the dopant, so in the case of carbon it is shifted off our scale. The electronic shell structure diminishes further in NMg_8 with two groupings of states, one subshell at −4 eV, and a very broad density of states from −2.5 eV to 1.5 eV, so broad that it can no longer be reasonably characterized as a subshell. With OMg_8 it is not possible to assign where one subshell may begin or end based simply on the density of states, indicating that a confined nearly free electron gas model is no longer sufficient to understand the electronic structure of OMg_8. FMg_8 has a different electronic structure, where there are well-defined F atomic orbitals and Mg orbitals, but minimal mixing between the two. As one progresses from Be towards F, the green regions indicating 2*p* dopant orbitals move deeper into the electronic structure from a strong hybridization between dopant *s*- and *p*-states and Mg states in $BeMg_8$ to a lone pair situation in OMg_8 and FMg_8 where the states with significant 2*p* density are primarily only 2*p* states. These variations in electronic structure as 2*p* electrons are added to the dopant atom show a strong evolution in electronic structure.

The key issue in the progression in electronic structure is the hybridization of the dopant electronic states with those of the Mg_8 cluster. To this end, we analyzed the nature of the electronic orbitals in each of the XMg_8 clusters. For each orbital, the angular momentum state was identified through inspection of the shapes of the orbitals and the nodes. The resulting analysis is shown in Figs. 4–6. We also show in Figs. S2 and S3 the orbital decomposition of the HOMO – 2, HOMO – 1, HOMO, LUMO, LUMO + 1, and LUMO + 2 electronic states to examine the orbital nature of the Frontier orbitals. Fig. S2(a) and S2(b) show the % contribution of the Mg s-and p-states while Figs S3(a) and S3(b) show the contribution of the X atom's s- and p- orbitals to these states. Note that the contribution of the Mg s-states to the orbitals generally decreases while that of the Mg p- orbitals generally increases as one goes from HOMO – 2 to LUMO + 2 showing that the p-states of Mg, that are unfilled in the atom, become occupied and contribute to orbitals near HOMO. Fig. S3(a) and S3(b) show that these Frontier states have contribution from p-states of the X atom and that the HOMO, HOMO – 1, and HOMO – 2 have negligible mixing of the X atom s-states.

We now focus on the progression of nature of the electronic states in the XMg_8 clusters. A Be atom has valence $2s^2$ state like $3s^2$ in Mg and the $BeMg_8$ presents an electronic spectrum that is best rationalized as a jellium set of states with

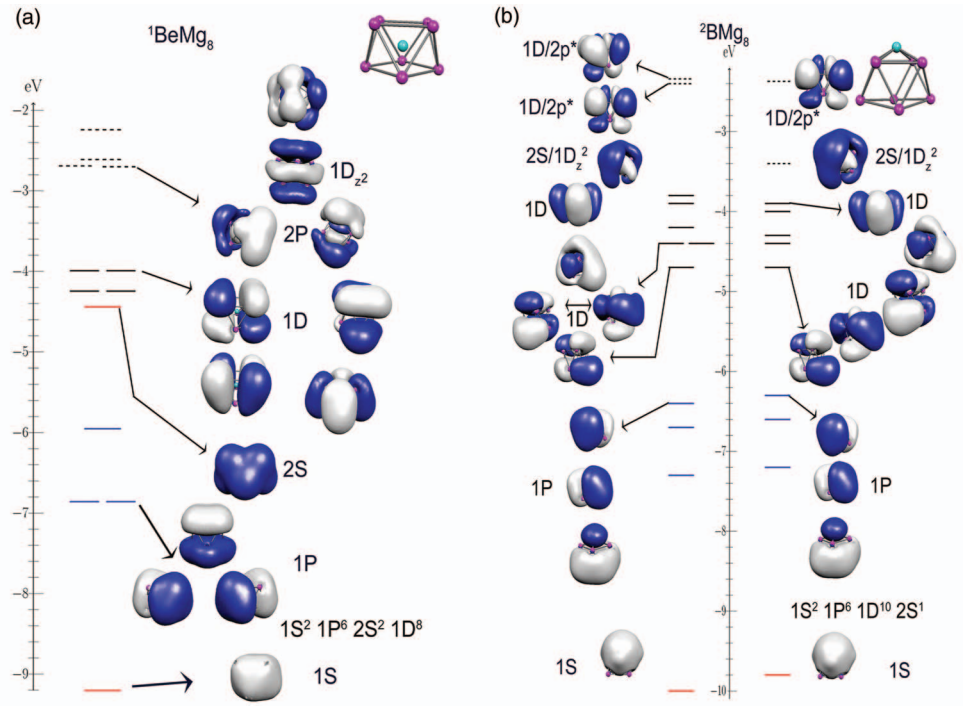

FIG. 4. (a) $BeMg_8$ and (b) BMg_8. The one electron energy levels and molecular orbital wavefunctions isosurfaces (isoval = 0.01 a.u.). The majority and minority levels are shown. Continuous lines correspond to the filled levels, whereas the dotted lines correspond to the unfilled states.

20 valence electrons shown in Fig. 4(a) composed of $|1S^2|\ 1P^6|\ 2S^2\ 1D^8\ ||\ 2P^4\ 1D_Z{}^2|$ superorbitals where the vertical lines indicate observed gaps and the double vertical line indicates the gap between filled and unfilled orbitals. Since the ground state geometry represents a compression along the z-axis, the $D_z{}^2$ orbital is split from the other D-states due to a crystal field splitting.[34,36] Consequently, while the cluster with 18 electrons has a configuration with a partially filled D shell, it is still quite stable with a large HOMO-LUMO gap of 1.29 eV through the crystal field splitting of the 1D subshell. The LUMO of $BeMg_8$ is an orbital assigned as two degenerate $2P^4$ orbitals. These orbitals are lower in energy than is expected for a NFE, but this can be understood more clearly as an antibonding orbital where the phase of the atomic 2*p*

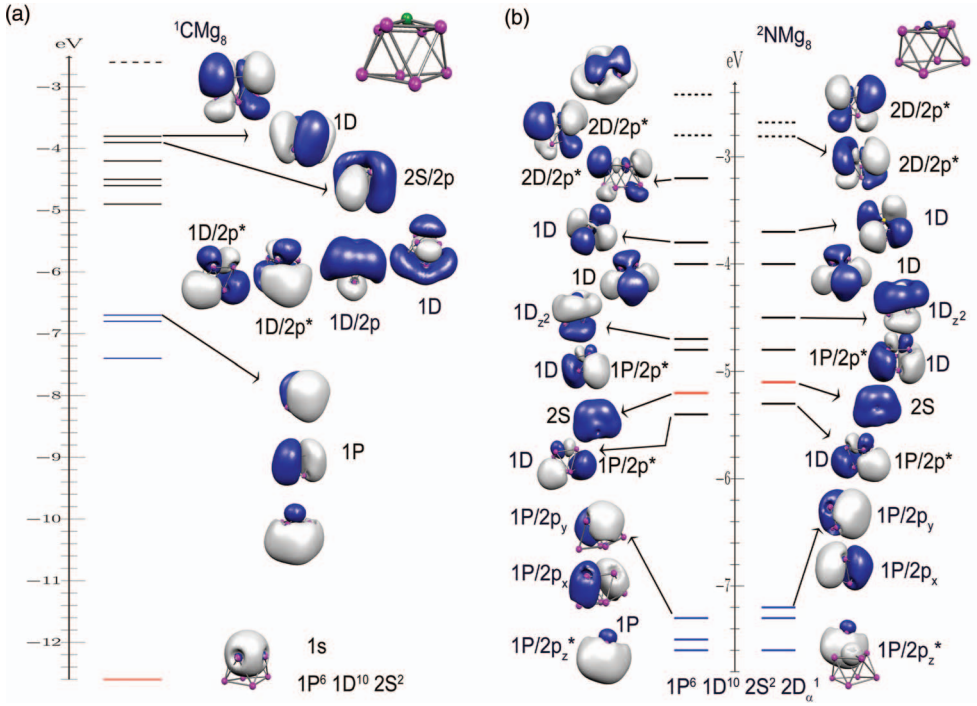

FIG. 5. (a) CMg_8 and (b) NMg_8. The one electron energy levels and orbital wavefunctions isosurfaces (isoval = 0.01 a.u.) are shown. See caption of Fig. 4.

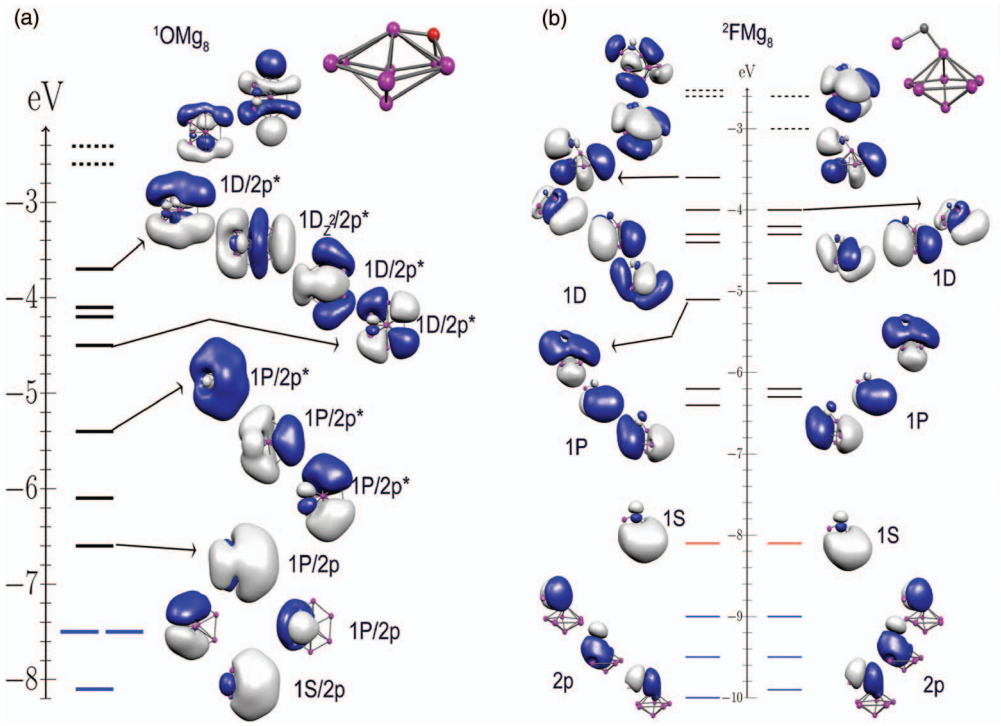

FIG. 6. (a) OMg_8 and (b) FMg_8. The one electron energy levels and orbital wavefunctions isosurfaces (isoval = 0.01 a.u.). See caption of Fig. 4.

orbital is reversed from that of the 2P NFE orbital. While both descriptions, 2P NFE and 1P/2*p**, can be adopted for the LUMO, the 1P/2*p** description is more consistent with the position of this orbital, as a 2P NFE orbital[34] is expected to be much higher in energy. The $1D_z^2$ orbital is found to be the LUMO + 2. We also note the importance of the conservation of symmetry in the hybridization of the impurity states with the Mg_8 orbitals.[52] The 2*s* atomic states of Be only mix with the $1S^2$ and $2S^2$ NFE orbitals, while the 2*p* atomic states mix exclusively with the $1P^6$ Mg_8 orbitals. As $BeMg_8$ is the only cluster studied here in which the dopant atom is endohedral, this is the only cluster where the symmetry of the atomic orbitals of the Be and the MO of the cluster have the same symmetry.

The BMg_8 is the first cluster with a dopant atom (B) with occupied valence *p*-orbitals ($2s^2$ $2p^1$). Note that we use capital letters to denote delocalized orbitals and lowercase to denote atomic orbitals. In the BMg_8 ground state, the B atom occupies an exterior site above the Mg plane. Fig. 4(b) shows the MO's of the BMg_8. The one-electron levels still have the expected subshell structure of a NFE model with 19 valence electrons, with assigned subshells of | $1S^2$ | $1P^6$ | $1D^{10}$ $2S^1$ || $2S^1$ | $2D^4$ |. Because the B atom is not in an endohedral position, the hybridization is different than that seen in $BeMg_8$. For example, the atomic 2s orbitals contribute to both 1S and $1P_z$ NFE orbitals because the B atom occupies an exterior site above the Mg plane placing it entirely in one lobe of the $1P_z$ orbital. Secondly, the NFE orbitals with the significant overlap with the 2*p* atomic orbitals now include the $1D_{xz}$ and $1D_{yz}$ orbitals in addition to the expected $1P_x$ and $1P_y$. This results in a significant amount of the 2*p* density of states now being found in the | $1D^{10}$ $2S^2$| shell. The cluster no longer has the oblate distortion of $BeMg_8$, so 2S and 1D orbitals are now found in the same shell. The LUMO + 1 is now a 1D/2*p** orbital, which is constructed from a 1D NFE orbital and a 2p atomic orbital that has opposing phase as indicated by the antibonding "star" which cannot be assigned using NFE notation.

The CMg_8 in Fig. 5(a) presents a similar electronic structure to BMg_8 as it also occupies a site above the Mg_4 plane. The 1*s* orbital of C is lower in energy and CMg_8 has an even number of electrons, but otherwise the DOS of the alpha channel of BMg_8 and CMg_8 are ostensibly the same. There is one small difference in that the C atom lies closer to the Mg_4 plane so that the $2p_z$ atomic orbital contributes primarily through the $1D_z^2$ NFE state in C, while in B the state with $2p_z$ contributions is assigned as 2S. D_z^2 and S orbitals belong to the same irreducible representation in all plausible point groups, so this difference is minor. Otherwise, the hybridization between the dopant atom and the Mg_8 cluster is strikingly similar in BMg_8 and CMg_8.

An alternative notation for the assignment of MO using the NFE subshell notation is one in which the character of the NFE orbital and atomic orbital are characterized as bonding or antibonding orbitals. We had previously used this description in unfilled orbitals, but as their inclusion was not necessary to describe the ground state electronic structure, we did not emphasize the point. Here we would like to emphasize that in many situations, the NFE and MO notation converge giving identical descriptions. For example, a $1P_x$ NFE orbital, and a $1P_x/2p_x$ are the same, $1P_x$ NFE orbital is constructed out of atomic orbitals, so one would expect contributions from the $2p_x$ atomic orbital to construct the expected $1P_x$ orbital. A second example is in the 1D NFE and 1P/2p* orbitals of CMg_8. In this orbital, the 1D and 1P/2p* descriptions are identical producing the 4 lobe orbital expected for 1D delocalized

orbital. This shows that the two conceptual models can converge to the same result in some cases. We raise this issue as NMg_8 is the first considered species where the ground state structure cannot be fully justified within a NFE description.

For NMg_8 in Fig. 5(b) the electronic structure retains some of the electronic structure of a jellium like picture, however the 2*p* orbitals of the N atom are deeper in energy and results in a larger perturbation of the electronic structure than the elements to its left on the periodic table. The 1P NFE states all have significant components from the N 2*p* orbitals. The lowest energy state may be thought of as a $1S/2p_z$ orbital where the node of the wave function is caused only by the N atom. The two other 1P NFE orbitals may also be assigned as 1P/2*p* orbitals, as the 2*p* atomic orbitals and 1P NFE orbitals belong to the same irreducible representation and have excellent overlap. The 1S/2*p* and 1P/2*p* orbitals are close in energy because they have the same number of nodes in the wave function and are constructed from the same 2*p* atomic orbital; this suggests that the molecular orbital notation is less useful than the NFE to predict the energy of these orbitals. The two lowest energy 1D NFE orbitals also have significant *p* components, in which the N atomic 2*p* orbitals act as the top two lobes of the $1D_{xz}$ and $1D_{yz}$ NFE orbitals, and they may be described as $1P_x/2p_x$* and $1P_y/2p_y$* in our molecular orbital notation. Note that these $1D_{xz}$ and $1D_{yz}$ orbitals were the HOMO of the $BeMg_8$ cluster, but are now over 2 eV below the HOMO showing the effect of the lower energy of the 2*p* nitrogen atomic orbitals. The orbital which lies 1.5 eV below the HOMO with A_1 symmetry is reminiscent of a $1D_z^2$; however, it may also be thought of as a $1P_z$ NFE orbital antibonding state with the $2p_z$ of N. Both of these heuristic aids explain the symmetry of the orbital, although the crystal field splitting of NFE predicts that this $1D_z^2$ would be the highest energy 1D orbital, while it is in fact the middle 1D NFE orbital. The next two orbitals are $1D_{xy}$ and $1D_{x^2-y^2}$ which are invariant to inversion, so they have no overlap with the N 2*p* orbitals by symmetry conservation. The HOMO of the NMg_8 can be best described as an antibonding orbital between the $1D_{xz}$ and $2p_x$ atomic orbitals showing that for NMg_8, the bonding picture between of atomic orbital and Mg_8 NFE orbitals is needed to describe all of the filled electronic orbitals in the cluster. We also note that the filling of the singly occupied antibonding orbital explains the decrease in the BE as we progress from C to N, as shown in Fig. 2. The large decrease in I.P. when moving from C to N also highlights the instability of this antibonding orbital.

Fig. 6(a) shows the energy levels and molecular orbitals for OMg_8. In this case the O atom leads to a distortion of the Mg_8 square antiprism to a hexagonal bipyramid with O bound to a triangular site. The 1S/2*p* and two 1P/2*p* orbitals are localized on the O site and show little separation from the remaining orbitals. The next three orbitals are assigned as 1P/2*p* and the next two as 1P/2*p**. These assignments are based on the wavefunction's nodes, in the Mg_8 unit and on its interaction with the O atom. At this point, a great deal of charge density has been placed on the O atom, so the remaining orbitals have smaller contributions from the O 2*p* orbitals. The remaining orbitals may be described as delocalized 2S and 1D orbitals but the 1D NFE orbitals have opposite phase with the 2*p* orbitals of the O atom, so they are assigned as 1D/2*p**. These orbitals are all very different from the predictions based on the jellium model, so the increased localization and deep 2*p* orbitals of O result in the molecular orbital picture giving more insight into the electronic structure.

The energy levels and molecular orbitals for FMg_8 shown in Fig. 6(b) present a completely different atomic structure where the F is bound to an apex atom. The 1S state is quite deep (and not shown in the figure) and the lowest *p*-states are completely localized on the F-site. The electronic spectrum is more aptly described as 2*p* atomic orbitals, followed by NFE orbitals with weak antibonding character with the F atom. This is marker for an ionic bond, and the charge transfer (NBO) from the Mg_8 motif to the F atom is $-0.99\ e^-$. As the interaction is ionic, the electronic structure may be split into two spaces and may be treated separately as atomic F orbitals and NFE orbitals of the Mg_8 which are strongly perturbed by the F atom.

In the above, we have shown above that XMg_8 clusters exhibit an interesting progression of hybridization between atomic and superatomic states. At the beginning of the series, the composite clusters may be aptly described using a metallic model to understand the electronic structure. As the number of 2*p* orbitals increases and their energy decreases hybridization between atomic and superatomic orbitals increases making the molecular orbital description more useful in understanding the electronic structure.

Hybridization between atomic and superatomic orbitals can also lead to interesting physical effects as shown in our recent work on XMg_8 clusters.[42] For these clusters, the atomic orbitals of significance are the 3*d*-states. The X atoms occupy an endohedral site within the Mg_8 square antiprism, and the symmetry enhances the hybridization between the atomic and superatomic states of D-character as they both belong to the same irreducible representation. The atomic 3*d*-states are marked by varying exchange splitting across the 3*d* series. As the *d*-states mix with superatomic D-shell, D-states are mostly affected by the atomic exchange splitting.

IV. CONCLUSIONS

The electronic structures of $BeMg_8$, BMg_8, and CMg_8 are found to be described following intuitive delocalized and localized concepts with small modifications due to the presence of the dopant atom. However as we change to dopant atoms with additional and lower energy 2*p* electrons such as NMg_8 and OMg_8, a molecular orbital picture which is more in line with a localized view of electronic structure provides more insight into the electronic structure, and allows for the qualitative assignment of orbitals. FMg_8 is even more localized, so orbitals may be viewed as primarily atomic or delocalized in nature. The molecular orbital concept may also be applied to work with magnetic dopants, as the symmetry of 3*d* localized and 1D delocalized orbitals are the same, so strong hybridization between these two orbitals may result in exchange splitting. The binding energy of the dopant increases monotonically from Be through C, and decreases to N, which is the first cluster with an occupied antibonding orbital between the dopant and the Mg_8 cluser orbitals.

Furthermore, there is a large decrease in ionization potential in NMg_8, indicating that this orbital interacts poorly with the Mg_8 cluster. Oxygen binds to the cluster most strongly, with extensive overlap between the deep 2p atomic orbitals and the cluster. The judicious use of these localized and delocalized concepts to understand cluster phenomenon shed light into the electronic structure of heteroatomic clusters.

ACKNOWLEDGMENTS

We gratefully acknowledge support from U. S. Department of Energy (DOE) through Grant No. DE-FG02-11ER16213.

[1]S. Shaik, New J. Chem. **31**, 2015 (2007).
[2]W. D. Knight, K. Clemenger, W. A. de Heer, W. A. Saunders, M. Y. Chou, and M. L. Cohen, Phys. Rev. Lett. **52**, 2141 (1984).
[3]S. N. Khanna and P. Jena, Phys. Rev. B **51**, 13705 (1995).
[4]M. Brack, Rev. Mod. Phys. **65**, 677 (1993).
[5]R. S. Mulliken, J. Chem. Phys. **3**, 375 (1935).
[6]J. E. Lennard-Jones, Trans. Faraday Soc. **25**, 668 (1929).
[7]P. Claes, E. Janssens, V. T. Ngan, P. Gruene, J. T. Lyon, D. J. Harding, A. Fielicke, M. T. Nguyen, and P. Lievens, Phys. Rev. Lett. **107**, 173401 (2011).
[8]E. Janssens, S. Neukermans, H. M. T. Nguyen, M. T. Nguyen, and P. Lievens, Phys. Rev. Lett. **94**, 113401 (2005).
[9]C. Romanescu, A. P. Sergeeva, W.-L. Li, A. I. Boldyrev, and L.-S. Wang, J. Am. Chem. Soc. **133**, 8646 (2011).
[10]W.-L. Li, C. Romanescu, T. R. Galeev, Z. A. Piazza, A. I. Boldyrev, and L.-S. Wang, J. Am. Chem. Soc. **134**, 165 (2011).
[11]L.-M. Wang, J. Bai, A. Lechtken, W. Huang, D. Schooss, M. M. Kappes, X. C. Zeng, and L.-S. Wang, Phys. Rev. B **79**, 033413 (2009).
[12]M. D. Deshpande, R. Pandey, M. A. Blanco, and A. Khalkar, J. Nanopart. Res. **12**, 1129 (2009).
[13]S. Zorriasatein, K. Joshi, and D. G. Kanhere, J. Chem. Phys. **128**, 184314 (2008).
[14]P. Chandrachud, K. Joshi, and D. G. Kanhere, Phys. Rev. B **76**, 235423 (2007).
[15]S. M. Ghazi and D. G. Kanhere, J. Phys. Chem. A **116**, 11 (2011).
[16]A. D. Zdetsis, J. Chem. Phys. **134**, 094312 (2011).
[17]B. Cao, A. K. Starace, C. M. Neal, M. F. Jarrold, S. Núñez, J. M. López, and A. Aguado, J. Chem. Phys. **129**, 124709 (2008).
[18]R. B. King, I. Silaghi-Dumitrescu, and M. M. Uta, J. Phys. Chem. A **115**, 2847 (2011).
[19]R. B. King, I. Silaghi-Dumitrescu, and M. M. Uta, Inorg. Chem. **48**, 8508 (2009).
[20]N. S. Bayliss, J. Chem. Phys. **16**, 287 (1948).
[21]H. Kuhn, J. Chem. Phys. **16**, 840 (1948).
[22]G. C. Pimentel and K. S. Pitzer, J. Chem. Phys. **17**, 882 (1949).
[23]R. Hoffmann and M. Gouterman, J. Chem. Phys. **36**, 2189 (1962).
[24]A. W. Castleman, Jr. and S. N. Khanna, J. Phys. Chem. C **113**, 2664 (2009).
[25]T. P. Martin, T. Bergmann, H. Göhlich, and T. Lange, Chem. Phys. Lett. **172**, 209 (1990).
[26]X. Li, H. Wu, X-B. Wang, and L.-S. Wang, Phys. Rev. Lett. **81**, 1909 (1998).
[27]G. Wrigge, M. A. Hoffmann, and B. v. Issendorff, Phys. Rev. A **65**, 063201 (2002).
[28]R. E. Leuchtner, A. C. Harms, and A. W. Castleman, Jr., J. Chem. Phys. **91**, 2753 (1989).
[29]O. C. Thomas, W. Zheng, S. Xu, and K. H. Bowen, Phys. Rev. Lett. **89**, 213403 (2002).
[30]A. C. Reber, S. N. Khanna, P. J. Roach, W. H. Woodward, and A. W. Castleman, Jr., J. Am. Chem. Soc. **129**, 16098 (2007).
[31]P. J. Roach, W. H. Woodward, A. W. Castleman, Jr., A. C. Reber, and S. N. Khanna, Science **323**, 492 (2009).
[32]A. C. Reber, S. N. Khanna, P. J. Roach, W. H. Woodward, and A. W. Castleman, Jr., J. Phys. Chem. A **114**, 6071 (2010).
[33]K. Clemenger, Phys. Rev. B **32**, 1359 (1985).
[34]P. J. Roach, W. H. Woodward, A. C. Reber, S. N. Khanna, and A. W. Castleman, Jr., Phys. Rev. B **81**, 195404 (2010).
[35]E. Janssens, S. Neukermans, and P. Lievens, Curr. Opin. Solid State Mater. Sci. **8**, 185 (2004).
[36]V. M. Medel, J. U. Reveles, A. C. Reber, S. N. Khanna, and A. W. Castleman, Jr., Phys. Rev. B **84**, 075435 (2011).
[37]D. E. Bergeron, A. W. Castleman, Jr., T. Morisato, and S. N. Khanna, Science **304**, 84 (2004).
[38]D. E. Bergeron, P. J. Roach, A. W. Castleman, Jr., N. O. Jones, and S. N. Khanna, Science **307**, 231 (2005).
[39]J. U. Reveles, S. N. Khanna, P. J. Roach, and A. W. Castleman, Jr., Proc. Natl. Acad. Sci. U.S.A. **103**, 18405 (2006).
[40]C. E. Jones, Jr., P. A. Clayborne, J. U. Reveles, J. J. Melko, U. Gupta, S. N. Khanna, and A. W. Castleman, Jr., J. Phys. Chem. A. **112**, 13316–13325 (2008).
[41]J. U. Reveles, P. A. Clayborne, A. C. Reber, S. N. Khanna, K. Pradhan, P. Sen, and M. R. Pederson, Nat. Chem. **1**, 310 (2009).
[42]V. M. Medel, J. U. Reveles, S. N. Khanna, V. Chauhan, P. Sen, and A. W. Castleman, Jr., Proc. Natl. Acad. Sci. U.S.A. **108**, 10062 (2011).
[43]V. Chauhan, V. M. Medel, J. Ulises Reveles, S. N. Khanna, and P. Sen, Chem. Phys. Lett. **528**, 39–43 (2012).
[44]M. Köster, P. Calaminici, M. E. Casida, V. D. Dominguez, R. Flores-Moreno, G. U. Gamboa, A. Goursot, T. Heine, A. Ipatov, F. Janetzko, J. M. del Campo, J. U. Reveles, A. Vela, B. Zuniga-Gutierrez, and D. R. Salahub, deMon2k Program, 2011.
[45]J. P. Perdew, K. Burke, and M. Ernzerhof, Phys. Rev. Lett. **77**, 3865 (1996).
[46]J. U. Reveles and A. M. Koster, J. Comp. Chem. **25**, 1109–1116 (2004).
[47]See supplementary material at http://dx.doi.org/10.1063/1.3700086 for the Cartesian coordinates of the ground states, and the geometries of the lowest energy isomers. The contribution of the *s* and *p* atomic orbitals for the dopant and Mg atoms to the molecular orbitals near the HOMO, are also included.
[48]P. H. Acioli and J. Jellinek, Phys. Rev. Lett. **89**, 213402-1–213402-4 (2002).
[49]K. Wade, Adv. Inorg. Chem. Radiochem. **18**, 1–66 (1976).
[50]D. M. P. Mingos, Nat. Phys. Sci. **236**, 99–102 (1972).
[51]D. M. P. Mingos, Acc. Chem. Res. **17**, 311–319 (1984).
[52]R. Hoffmann and R. B. Woodward, Acc. Chem. Res. **1**, 17 (1968).